

PAPER

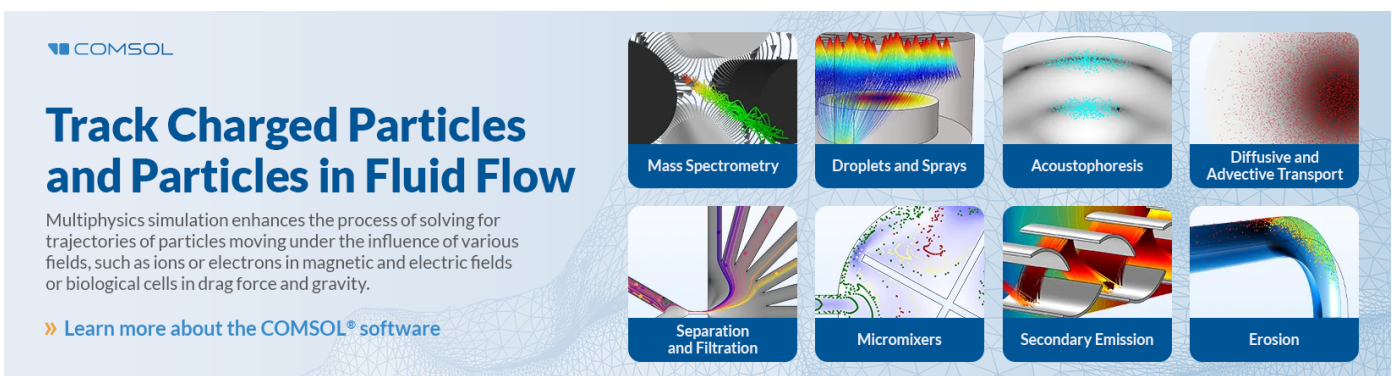
# Anisotropy and paramagnetism of QCD matter with an anomalous magnetic moment

To cite this article: Rui He and Xin-Jian Wen 2024 *J. Phys. G: Nucl. Part. Phys.* **51** 065001

View the [article online](#) for updates and enhancements.

## You may also like

- [The dynamical holographic QCD method for hadron physics and QCD matter](#)  
Yidian Chen, Danning Li and Mei Huang
- [The exploration of hot and dense nuclear matter: introduction to relativistic heavy-ion physics](#)  
Hannah Elfner and Berndt Müller
- [Probing dense QCD matter in the laboratory—The CBM experiment at FAIR](#)  
P Senger and for the CBM Collaboration

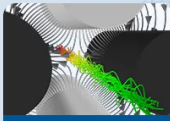
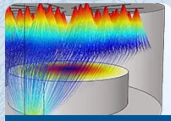
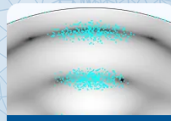
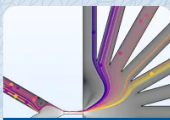
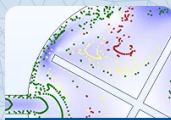
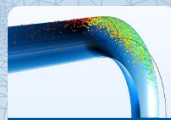


**COMSOL**

## Track Charged Particles and Particles in Fluid Flow

Multiphysics simulation enhances the process of solving for trajectories of particles moving under the influence of various fields, such as ions or electrons in magnetic and electric fields or biological cells in drag force and gravity.

» [Learn more about the COMSOL® software](#)

 Mass Spectrometry	 Droplets and Sprays	 Acoustophoresis	 Diffusive and Advective Transport
 Separation and Filtration	 Micromixers	 Secondary Emission	 Erosion

# Anisotropy and paramagnetism of QCD matter with an anomalous magnetic moment

Rui He  and Xin-Jian Wen 

Institute of Theoretical Physics, State Key Laboratory of Quantum Optics and Quantum Optics Devices, Shanxi University, Taiyuan, Shanxi 030006, People's Republic of China

E-mail: [heruimm@qq.com](mailto:heruimm@qq.com)

Received 5 December 2023, revised 8 March 2024

Accepted for publication 21 March 2024

Published 22 April 2024



CrossMark

## Abstract

We employ the Polyakov-loop enhanced Nambu–Jona-Lasinio model incorporating the quark anomalous magnetic moment to investigate the anisotropy structure and the renormalized magnetization of magnetized quark matter at finite temperature. The ultraviolet divergences and nonphysical oscillatory behavior are eliminated by the vacuum magnetic regularization scheme. With a parametrization of the anomalous magnetic moment that is proportional to the square of the chiral condensate, the renormalized magnetization is enlarged by the strong magnetic field so that the anisotropy becomes more apparent. The inflection point of the renormalized magnetization indicates the pseudo-critical temperature for the chiral crossover. We find that the results with the anomalous magnetic moment are closer to the lattice quantum chromodynamics data. The connection between the paramagnetism and the chiral transition provides new insight into a magnetohydrodynamics description of hot and dense QCD matter produced in heavy-ion collisions.

Keywords: anisotropy, paramagnetism, QCD matter, anomalous magnetic moment, polyakov loop enhanced nambu- jona-lasinio model

## 1. Introduction

In recent years, there has been great interest in the nature of the phase diagram of quantum chromodynamics (QCD) matter, especially the thermodynamic and magnetic properties in the presence of both a heat bath and strong magnetic fields. Neutron stars are widely believed to

possess strong magnetic fields and can exhibit surface magnetic fields reaching magnitudes of  $10^{14} \sim 10^{15}$  Gauss [1–6]. In the early Universe, primordial magnetic fields even as high as  $10^{23}$  Gauss may have arisen during electroweak phase transition driven by a chiral anomaly [7, 8]. Strong magnetic fields with strengths around  $10^{19}$  Gauss can be produced in heavy-ion collision experiments. A comprehensive understanding of the bulk and microscopic properties of magnetized QCD matter becomes crucial for revealing various physical phenomena, including the magnetars and the heavy-ion collision experiments. Recently, extensive attention has been devoted to numerical simulations of lattice QCD (LQCD) and analytical model approximations [9–20]. These investigations primarily focus on the influence of magnetic fields on the equations of state of the matter composing the star, encompassing hadronic matter, quark matter and hybrid stars matter [21–26].

Due to the spatial asymmetry introduced by the magnetic field in the  $z$ -direction, the pressure becomes different in the parallel and perpendicular directions, corresponding to the spatial components of the energy-momentum tensor [27]. In reality, depending on the magnitude of the magnetic field, the parallel pressure becomes much smaller than the perpendicular pressure. The anisotropy was first introduced by Ferrer *et al* [28] and is related to the magnetization of the magnetized matter [29]. Therefore, many studies have aimed to investigate the effects of magnetic fields on the anisotropic equation of state of compact stars, such as neutron stars, quark stars and hybrid stars [9, 30–34].

The investigation of the quark anomalous magnetic moment (AMM) has received considerable attention. The study goes through several important stages in the literature. In the 1980s, it was first shown that the larger light-quark AMM is significant when checking the experimental consequences for the quark mass generation in the dynamical breaking of chiral symmetry [35]. In the massless current quark mass, the breaking of chiral symmetry could trigger the generation of a quark AMM [36]. The AMM correlated to the transversity was large enough not to be ignored. By including the AMM, the magnetization would have a different form [37]. In further exploration of the complete portrait of the QCD diagram, the inverse magnetic catalysis (IMC) effect was observed for a larger AMM [38]. In a strong magnetic field, the AMM was found to decrease with the increasing Landau level and would make an insignificant contribution to the equation of state [33]. Later, numerous studies were dedicated to exploring the influence of the AMM on the chiral restoration and deconfinement-phase transition of QCD matter in strong magnetic fields [39–42]. The AMM is widely accepted to account for the IMC, as initially proposed by LQCD results [43]. Recently, the constant AMM and the AMM that is proportional to the chiral condensate have been proven to be inappropriate forms [44]. The AMM that is proportional to the square of the chiral condensate was suggested to yield the chiral condensate as functions of the temperature and magnetic field, which is in excellent agreement with LQCD results [44]. It is believed that the scale of the AMM plays a significant role in introducing the IMC effect in the vicinity of the critical temperature [39, 45].

The Nambu–Jona-Lasinio (NJL) model offers a framework for describing nucleons and mesons as a low-energy effective theory of QCD. It has also been proposed as a valuable model for describing the QCD chiral symmetry and the vacuum spontaneous breakdown in the presence of strong magnetic fields at finite density and/or temperature [46, 47]. However, the NJL model cannot describe the deconfinement-phase transition of QCD matter. Therefore, in the Polyakov-loop enhanced NJL (PNJL) model, the Polyakov loop can be used as an approximate order parameter for the deconfinement transition associated with the spontaneous symmetry breaking of the center symmetry. The presence of four-fermion interactions in the PNJL model leads to nonrenormalizability, and an appropriate regularization scheme is needed to avoid ultraviolet divergences. Recently, a new method called the vacuum magnetic

regularization (VMR) scheme has been proposed [48–50], offering a successful description of the thermomagnetic properties of QCD matter. This scheme separates the potential divergences in pure vacuum from the finite magnetic contributions. The VMR scheme is not only able to eliminate the unphysical oscillatory behavior in chiral quark condensate or tachyonic neutral pion masses that are observed when using the non-magnetic-field independent regularization (non-MFIR) scheme [51], but can also achieve the paramagnetism of QCD matter [52]. In our present work, we employ the VMR scheme to regularize the thermodynamic potential divergence. Our goal is to investigate the effect of the quark AMM on the anisotropy pressures and paramagnetism of QCD matter at finite temperatures. Specifically, the effect of the AMM on the renormalized magnetization of QCD matter will be studied using different AMM scales.

The paper is organized as follows. In section 2, we present the thermodynamics of the three-flavor PNJL model at finite temperature in a strong magnetic field. In section 3, the numerical results are shown with a detailed analysis of the influence of the AMM on anisotropy pressures and paramagnetism. The last section is a short summary.

## 2. Thermodynamics of the SU(3) PNJL model at finite temperature

In the SU(3) version of the PNJL model under a strong magnetic field, the Lagrangian density is given by

$$\begin{aligned} \mathcal{L}_{\text{PNJL}} = & \bar{\psi}(i\not{D} - m + \gamma^0\mu_q + \frac{1}{2}\hat{a}\sigma^{\mu\nu}F_{\mu\nu})\psi + G\sum_{a=0}^8[(\bar{\psi}\lambda_a\psi)^2 + (\bar{\psi}i\gamma_5\lambda_a\psi)^2] - K[\det\bar{\psi}(1 + \gamma_5)\psi \\ & + \det\bar{\psi}(1 - \gamma_5)\psi] - U(\Phi, \bar{\Phi}, T), \end{aligned} \quad (1)$$

where  $\psi$  is the quark field and carries three flavors ( $u$ ,  $d$  and  $s$  quarks), and  $\lambda_a$  ( $a = 1, \dots, N_f^2 - 1$ ) represents the SU(3) Gell-Mann matrices in the three-flavor space. The covariant derivative with the magnetic field is introduced as  $\not{D} \sim \gamma^\mu D_\mu$  and  $D_\mu = \partial_\mu - ie\hat{Q}A_\mu$ . The charge matrix is given by  $\hat{Q} \equiv \text{diag}(q_u, q_d, q_s) = \text{diag}(2/3, -1/3, -1/3)$ . The abelian gauge field  $A_\mu$  stands for the external magnetic field  $B$  aligned along the  $z$ -direction. The AMM is introduced by the  $\sigma^{\mu\nu} = i[\gamma^\mu, \gamma^\nu]/2$  coupling with the electromagnetic field strength  $F^{\mu\nu} = \partial^\mu A^\nu - \partial^\nu A^\mu$ . The metric tensor used in this work is  $g^{\mu\nu} = \text{diag}(1, -1, -1, -1)$ . The factor  $\hat{a} = \hat{Q}\hat{\kappa}$  is defined, where  $\hat{\kappa} = \text{diag}(\kappa_u, \kappa_d, \kappa_s)$  is a  $3 \times 3$  matrix in the flavour space, and  $\kappa_i$  are the AMMs of the different flavors. The more recent results suggested that the proper form of the AMM would change with the chiral condensate, since it involves the behavior related to the condensate [44]. The potential  $U(\Phi, \bar{\Phi}, T)$  in the Lagrangian equation (1) governs the dynamics of the traced Polyakov loop and its conjugate and is given by

$$U(\Phi, \bar{\Phi}, T) = -\frac{b_2(T)}{2}\bar{\Phi}\Phi - \frac{b_3}{6}(\Phi^3 + \bar{\Phi}^3) + \frac{b_4}{4}(\bar{\Phi}\Phi)^2 \quad (2)$$

where

$$b_2(T) = a_0 + a_1\left(\frac{T_0}{T}\right) + a_2\left(\frac{T_0}{T}\right)^2 + a_3\left(\frac{T_0}{T}\right)^3. \quad (3)$$

The coefficients are given in table 1 [53]. Following the argument in [54], we have chosen the critical Polyakov temperature  $T_0 = 187$  MeV.

**Table 1.** The parameter set for the Polyakov potential.

$a_0$	$a_1$	$a_2$	$a_3$	$b_3$	$b_4$
6.75	-1.95	2.625	-7.44	0.75	7.5

The thermodynamic potential for a three-flavor PNJL model is expressed as

$$\Omega = \sum_i \Omega_i + 2G \sum_i \sigma_i^2 - 4K \sigma_u \sigma_d \sigma_s + U(\Phi, \bar{\Phi}, T), \quad (4)$$

where  $\Omega_i = \Omega_i^{\text{vac}} + \Omega_i^{\text{field}} + \Omega_i^{\text{mag}} + \Omega_i^{\text{med}}$ . The contributions  $\Omega_i^{\text{vac}}$  and  $\Omega_i^{\text{field}}$  must be regularized and the following expressions are given by [50]

$$\Omega_i^{\text{vac}} = -\frac{N_c}{8\pi^2} \left\{ \Lambda [\Lambda^2 + \epsilon_i^2(\Lambda)] \epsilon_i(\Lambda) - K_{0i}^4 \ln \left[ \frac{\Lambda + \epsilon_i(\Lambda)}{K_{0i}} \right] \right\}, \quad (5)$$

$$\Omega_i^{\text{field}} = -\frac{N_c B_i^2}{48\pi^2} [3(\alpha_i + 1)^2 - 1] \ln \frac{K_{0i}^2}{\Lambda^2}, \quad (6)$$

where the ultraviolet divergence is regularized by the 3D sharp cutoff scheme. The definitions  $K_{0i} = \sqrt{M^2 + \kappa_i^2 B_i^2}$  and  $\epsilon_i^2(\Lambda) = K_{0i}^2 + \Lambda^2$  are adopted to include the AMM with the parameter  $B_i$  defined as  $B_i = q_{ie} B$ . The magnetic field contribution  $\Omega_i^{\text{mag}}$  is [50],

$$\Omega_i^{\text{mag}} = \frac{N_c}{8\pi^2} \int_0^\infty \frac{ds}{s^3} e^{-sK_{0i}^2} \left\{ \frac{B_i s \cosh[(\alpha_i + 1)B_i s]}{\sinh(B_i s)} - 1 - \frac{1}{6} [3(\alpha_i + 1)^2 - 1] (B_i s)^2 \right\}, \quad (7)$$

with the notation  $\alpha_i = 2M\kappa_i$ . The contribution of the medium  $\Omega_i^{\text{med}}$  at finite temperature is [50],

$$\Omega_i^{\text{med}} = -T \frac{N_c |B_i|}{4\pi^2} \sum_{n=0}^\infty \sum_{s=\pm 1} \int_{-\infty}^\infty dp_z [\ln(g^+) + \ln(g^-)]. \quad (8)$$

The quantities  $g^+$  and  $g^-$  are defined as

$$g^+ = 1 + 3(\Phi + \bar{\Phi} e^{-\frac{E_{nis} - \mu_q}{T}}) e^{-\frac{E_{nis} - \mu_q}{T}} + e^{-3\frac{E_{nis} - \mu_q}{T}}, \quad (9)$$

$$g^- = 1 + 3(\bar{\Phi} + \Phi e^{-\frac{E_{nis} + \mu_q}{T}}) e^{-\frac{E_{nis} + \mu_q}{T}} + e^{-3\frac{E_{nis} + \mu_q}{T}}. \quad (10)$$

The quark energy eigenvalue  $E_{nis}$  is influenced by the AMM in the effective quantity as

$$E_{nis} = \sqrt{p_z^2 + (M_{nis} - sT_i)^2}, \quad (11)$$

and  $M_{nis}$  is defined as

$$M_{nis} = \sqrt{\left( 2n + 1 - s \frac{q_i}{|q_i|} \right) |B_i| + M^2}. \quad (12)$$

where  $T_i = \kappa_i B_i$  includes the AMM according to the Schwinger linear ansatz [55],  $n$  is the Landau level (LL) number and  $s = \pm 1$  stands for the spin of the quark. The AMM separates the energies of the up and down spin in the LL ( $n \neq 0$ ), in addition to the lowest Landau level (LLL) ( $n = 0$ ).

By using the following stationary conditions,

$$\frac{\partial\Omega}{M} = 0; \quad \frac{\partial\Omega}{\Phi} = 0; \quad \frac{\partial\Omega}{\bar{\Phi}} = 0; \quad (13)$$

we can obtain the following sets of coupled gap equations

$$\begin{aligned} M_u &= m_u - 4G\sigma_u + 2K\sigma_d\sigma_s, \\ M_d &= m_d - 4G\sigma_d + 2K\sigma_u\sigma_s, \\ M_s &= m_s - 4G\sigma_s + 2K\sigma_u\sigma_d, \end{aligned} \quad (14)$$

$$\left\{ -\frac{b_2(T)}{2}\bar{\Phi} - \frac{b_3}{2}\bar{\Phi}^2 + \frac{b_4}{2}(\bar{\Phi}\Phi)\bar{\Phi} \right\} - \frac{3}{T^3} \sum_{nis} \frac{B_i}{2\pi^2} \int_0^\infty dp_z \left[ \frac{e^{-\frac{E_{nis}-\mu_q}{T}}}{g^+} + \frac{e^{-2\frac{E_{nis}+\mu_q}{T}}}{g^-} \right] = 0, \quad (15)$$

$$\left\{ -\frac{b_2(T)}{2}\Phi - \frac{b_3}{2}\Phi^2 + \frac{b_4}{2}(\bar{\Phi}\Phi)\Phi \right\} - \frac{3}{T^3} \sum_{nis} \frac{B_i}{2\pi^2} \int_0^\infty dp_z \left[ \frac{e^{-2\frac{E_{nis}-\mu_q}{T}}}{g^+} + \frac{e^{-\frac{E_{nis}+\mu_q}{T}}}{g^-} \right] = 0, \quad (16)$$

where the chiral condensate equals  $\sigma_i = \sigma_i^{\text{vac}} + \sigma_i^{\text{field}} + \sigma_i^{\text{mag}} + \sigma_i^{\text{med}}$ . The terms  $\sigma_i^{\text{vac}}$ ,  $\sigma_i^{\text{field}}$  and  $\sigma_i^{\text{mag}}$  represent the vacuum, the field and the magnetic field to the quark condensate, respectively. The regularized vacuum contribution reads [50]

$$\sigma_i^{\text{vac}} = -\frac{MN_c}{2\pi^2} \left\{ \Lambda\epsilon_i(\Lambda) - K_{0i}^2 \ln \left[ \frac{\Lambda + \epsilon_i(\Lambda)}{K_{0i}} \right] \right\}, \quad (17)$$

The finite magnetic-field-dependent contributions are given by [50]

$$\sigma_i^{\text{field}} = -\frac{MN_c B_i^2 [3(\alpha_i + 1)^2 - 1]}{24\pi^2 K_{0i}^2}, \quad (18)$$

$$\begin{aligned} \sigma_i^{\text{mag}} &= \\ & -\frac{MN_c}{4\pi^2} \int_0^\infty \frac{ds}{s^2} e^{-sK_{0i}^2} \left\{ \frac{B_i s \cosh[(\alpha_i + 1)B_i s]}{\sinh(B_i s)} - 1 - \frac{1}{6} [3(\alpha_i + 1)^2 - 1] (B_i s)^2 \right\}. \end{aligned} \quad (19)$$

And  $\sigma_i^{\text{med}}$  is the contribution of the thermal medium in the following expression [50]

$$\sigma_i^{\text{med}} = \frac{MN_c |B_i|}{4\pi^2} \sum_{n=0}^\infty \sum_{s=\pm 1} \int_{-\infty}^\infty \frac{dp_z}{E_{nis}} (f^+ + f^-) \left( 1 - \frac{sT_i}{M_{nis}} \right), \quad (20)$$

where the fermion distribution function is defined as

$$f^+ = \frac{(\Phi + 2\bar{\Phi} e^{-\frac{E_{nis}-\mu_q}{T}}) e^{-\frac{E_{nis}-\mu_q}{T}} + e^{-3\frac{E_{nis}-\mu_q}{T}}}{g^+}, \quad (21)$$

$$f^- = \frac{(\bar{\Phi} + 2\Phi e^{-\frac{E_{nis}+\mu_q}{T}}) e^{-\frac{E_{nis}+\mu_q}{T}} + e^{-3\frac{E_{nis}+\mu_q}{T}}}{g^-}. \quad (22)$$

According to the LQCD evaluations, the QCD vacuum is paramagnetic at  $T=0$ . Due to the quantization, the magnetization cannot be determined as the partial derivative of the parallel pressure with respect to the  $B$ . Therefore, it has shown the paramagnetism by

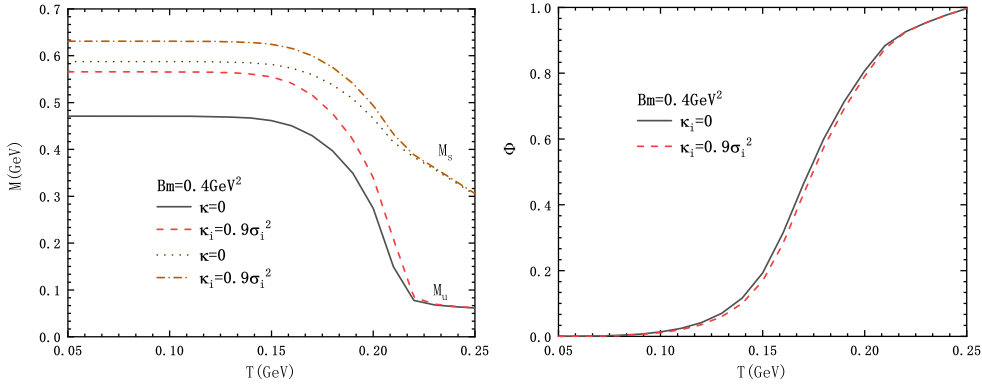


**Figure 1.**  $M$  (left panel) and  $\Phi$  (right panel) as a function of temperature for the same magnetic field at the AMMs  $\kappa_i = 0$  and  $\kappa_i = 0.9\sigma_i^2$ .

introducing the renormalized magnetization  $\mathcal{M}^r$  as [27],

$$\mathcal{M}^r \cdot eB = \mathcal{M} \cdot eB - (eB)^2 \lim_{eB \rightarrow 0} \frac{\mathcal{M} \cdot eB}{(eB)^2} \Big|_{r=0}, \quad (23)$$

where the magnetization is defined as  $\mathcal{M} = \frac{\partial P_{\parallel}}{\partial B}$ , the parallel pressure is the negative thermodynamic potential  $P_{\parallel} = -\Omega$ , and the transverse pressure is subjected to the extra contribution  $P_{\perp} = P_{\parallel} - \mathcal{M}B$  due to the quantization of the charged particles in Landau levels. In the PNJL model, the evaluations with  $\mathcal{M}$  cannot be consistent with the paramagnetic feature from the LQCD results. To address this shortcoming, the renormalized magnetization is presented in the VMR scheme as [48],

$$\mathcal{M}^r = \frac{\partial P_{\parallel}^r}{\partial B}, \quad (24)$$

where  $P_{\parallel}^r$  is the renormalized pressure, which is defined as [48],

$$P_{\parallel}^r = P_{\parallel} - (eB)^2 \lim_{eB \rightarrow 0} \frac{P_{\parallel}}{(eB)^2} \Big|_{r=0}. \quad (25)$$

It has been shown that the paramagnetism can be reproduced by introducing the renormalized magnetization  $\mathcal{M}^r$  in the PNJL model.

### 3. Numerical results and discussion

In this section, the AMM effect on the anisotropy at finite temperature is studied in the strong magnetic field. The paramagnetism of the bulk matter is reproduced and influenced by the scale of the AMM. In the present calculation, the following parameters are adopted:  $m_u = m_d = 5.5$  MeV,  $m_s = 135.7$  MeV,  $\Lambda = 631.4$  MeV,  $G = 1.835/\Lambda^2$  and  $K = 9.29/\Lambda^5$  [56]. The AMMs for  $u$ ,  $d$  and  $s$  quarks are used:  $\kappa_i = v\sigma_i^2$  ( $i = u, d, s$ ) [44]. The quark dynamical mass  $M$  as a function of magnetic fields at different temperatures can be obtained by solving the gap equations: equations (14), (15) and (16). Then we can obtain the anisotropic pressure and renormalized magnetization of magnetized quark matter by substituting the  $\mathcal{M}$  into equation (24). In our calculations, we assume a scenario in that the chemical potential for both the up, down and the strange quark ( $\mu_u$ ,  $\mu_d$  and  $\mu_s$ ) are zero.

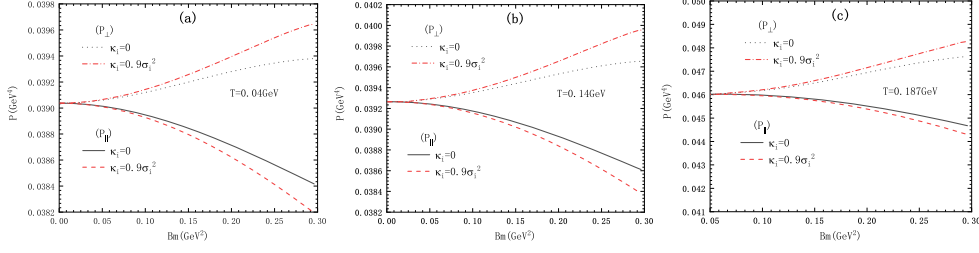


**Figure 2.** The behavior of the longitudinal pressure and the transverse pressure for different temperatures as a function of the magnetic field with and without AMMs at (a)  $T = 0.04\text{ GeV}$ , (b)  $T = 0.14\text{ GeV}$  and (c)  $T = 0.187\text{ GeV}$ .

Figure 1 shows the quark dynamical mass  $M$  as an order parameter for the chiral-phase transition (left panel) and the expectation value of the Polyakov loop  $\Phi$  as an order parameter for the deconfinement-phase transition (right panel). Chiral restoration and the deconfinement-phase transition happen at high temperatures. There are two different AMM values,  $\kappa_i = 0$  and  $\kappa_i = 0.9\sigma_i^2$ , at a fixed magnetic field,  $Bm = 0.4\text{ GeV}^2$ . The quark dynamical mass  $M$  of  $u$  and  $s$  quarks are manifested as decreasing smooth functions of temperatures at  $\kappa_i = 0$  and  $\kappa_i = 0.9\sigma_i^2$ , which indicates a chiral crossover. The quark dynamical mass  $M$  is apparently enhanced by increasing AMMs. The data indicate a 20% increase for  $M_u$  and a 7% increase for  $M_s$  compared to the zero AMM at  $T = 0.05\text{ GeV}$ . As the temperature increases, the effect of the AMM gradually weakens until it almost disappears. This means that there is a more obvious impact on quark dynamical mass at low temperatures. In the right panel, we observed a 6% increase in deconfinement temperatures compared to the  $\kappa_i = 0$ .

In figure 2, the anisotropic pressure is shown as a function of the magnetic field at different temperatures, respectively, in three panels: (a)  $T = 0.04\text{ GeV}$  for the chiral symmetry breaking phase, (b)  $T = 0.14\text{ GeV}$  near the phase transition point, and (c)  $T = 0.187\text{ GeV}$  in the chiral restoration. For the convenience of comparison, the two different AMM values  $\kappa_i = 0$  and  $\kappa_i = 0.9\sigma_i^2$  are marked by the red and black curves, respectively. In panels (a) and (b), it is obvious that the presence of the nonzero AMM slightly enhances the growth of the transverse pressure, inversely leading to a reduction in the longitudinal pressure. It exhibits a change of approximately 5% at  $Bm = 0.3\text{ GeV}^2$ . Although the change seems insignificant, it is concluded that the AMM enhances the splitting of the pressures parallel and transverse to the magnetic field direction. The anisotropy of the quark matter is consistent with the results reported in [37, 51]. However, in panel (c), the two AMM cases are nearly indistinguishable in the chiral restoration due to our ansatz that the AMM is proportional to the square of the quark condensate. The high temperature results in a decrease in the quark condensate as well as the value of the AMM. Consequently, it can be concluded that the effect of the AMM is more prominent and observable in lower-temperature regions.

In figure 3, the longitudinal pressures in the left panel and the transverse pressures in the right panel are shown as functions of the temperature at a fixed magnetic field  $Bm = 0.15\text{ GeV}^2$ . The different scales of the AMM are indicated by the different coefficients 0, 0.5 and 0.9. By comparing the data at  $T = 0.05\text{ GeV}$ , we found a change of approximately 0.06% at  $\kappa_i = 0.5\sigma_i^2$  and 0.1% at  $\kappa_i = 0.9\sigma_i^2$ . It is shown that the AMM increases, and the value of the longitudinal pressure decreases as the coefficient increases. Conversely, for the transverse pressures, the transverse pressure increases as the coefficient increases. This observation indicates that the presence of the AMM can indeed enhance the pressure anisotropies in quark matter. Furthermore, it is noteworthy that the larger the value of the AMM, the more

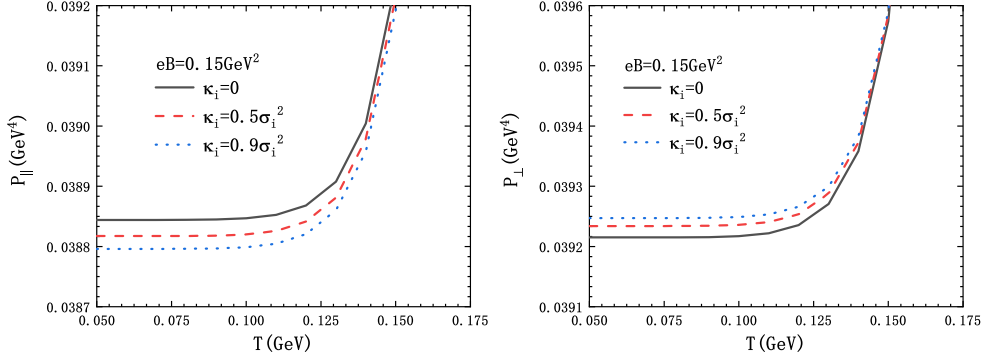


**Figure 3.** The  $P_{\parallel}$  (left panel) and  $P_{\perp}$  (right panel) as a function of temperature for the same magnetic field at the AMMs  $\kappa_i = 0$ ,  $\kappa_i = 0.5\sigma_i^2$  and  $\kappa_i = 0.9\sigma_i^2$ .

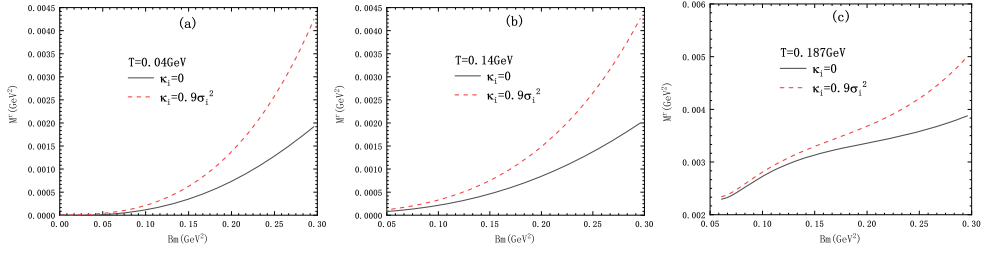


**Figure 4.** The behavior of the renormalized magnetization for different temperatures as a function of the magnetic field with and without AMMs at (a)  $T = 0.04\text{GeV}$ , (b)  $T = 0.14\text{GeV}$  and (c)  $T = 0.187\text{GeV}$ .

pronounced the level of pressure anisotropies becomes. Similarly, in the two panels, we can clearly observe that the effect of the AMM on the pressure anisotropies becomes less important as the temperature increases. In general, for a fixed magnetic field and at low temperatures, it can be concluded that a larger AMM value leads to a more visible change in the anisotropic pressures.

As discovered in [48], the renormalized magnetization within the VMR scheme is demonstrated as an effective approach to account for the magnetic characteristics of QCD vacuum. In figure 4, the renormalized magnetization is shown as a function of the magnetic field in three panels:  $T = 0.04$ ,  $0.14$  and  $0.187\text{ GeV}$ . The AMM values  $\kappa_i = 0$  and  $0.9\sigma_i^2$  are marked by the solid and dashed curves, respectively. The paramagnetism is displayed by the positive renormalized magnetization  $\mathcal{M}^r$ , which is in agreement with the results of LQCD [27]. The renormalized magnetization increases with the magnetic field strength. The difference between the solid and dashed curve is becoming larger as the magnetic field increases. It is apparent that the increasing magnetic field leads to the more pronounced effect of the AMM. At  $Bm = 0.3\text{ GeV}^2$ , the presence of the nonzero AMM will increase the renormalized magnetization up to one time in panels (a) and (b), and one half in panel (c). It is concluded that as the temperature goes up to the critical value, the influence of the AMM on the renormalized magnetization becomes less pronounced. Moreover, the ascendant trend of  $\mathcal{M}^r$  with the magnetic field behaves like a linear increasing function for the chiral symmetric matter.

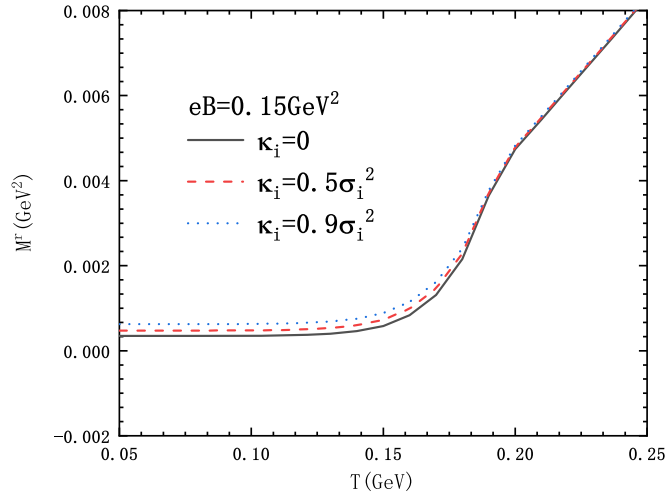


**Figure 5.** The renormalized magnetization as a function of temperature for the same magnetic field at the AMMs  $\kappa_i = 0$ ,  $\kappa_i = 0.5\sigma_i^2$  and  $\kappa_i = 0.9\sigma_i^2$ .

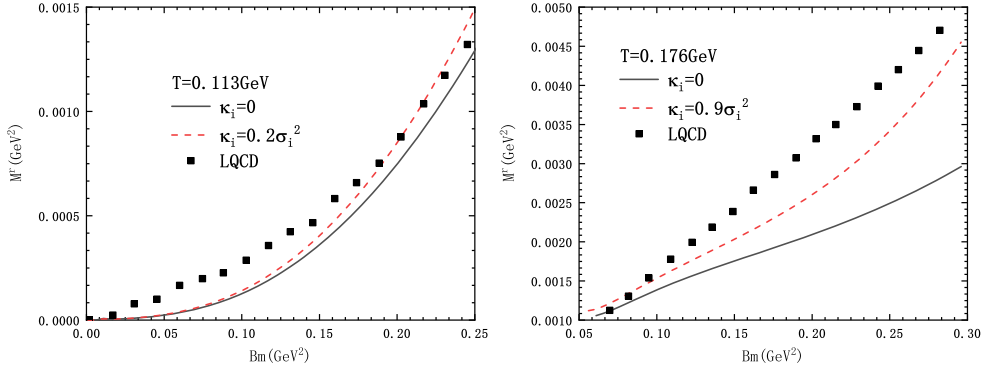


**Figure 6.** The renormalized magnetization  $M^r$  as a function of the magnetic field for two sets of temperatures:  $T = 0.113$  GeV (left panel) at the AMMs  $\kappa_i = 0$  and  $\kappa_i = 0.2\sigma_i^2$ , and  $T = 0.176$  GeV (right panel) at the AMMs  $\kappa_i = 0$  and  $\kappa_i = 0.9\sigma_i^2$ . The black dotted line represents the fit for the LQCD results [57].

In figure 5, the renormalized magnetization is shown as an increasing function of temperature at a fixed magnetic field  $eB = 0.15$  GeV<sup>2</sup>. It can be understood that the more Landau levels there are at high temperature, the stronger the magnetization. The zero AMM is marked by the solid line. And the nonzero AMMs  $\kappa_i = 0.5, 0.9\sigma_i^2$  are marked by the dashed line, the dotted and the dash-dotted curves, respectively. By comparing the three curves at  $T = 0.05$  GeV, we found a change of approximately 36.8% at  $\kappa_i = 0.5\sigma_i^2$  and 80.2% at  $\kappa_i = 0.9\sigma_i^2$ . It is shown that the increase in the AMM coefficient leads to a larger renormalized magnetization at lower temperatures far away from the critical point. However, as the temperature increases, the effect of the AMM on the renormalized magnetization becomes so weak that the three lines overlap with the solid line. Moreover, the inflection point of the renormalized magnetization indicates the pseudocritical temperature for the chiral crossover. This implies that

the scale of AMM that is proportional to the chiral condensate is so meaningful for revealing a chiral signal shown by the behavior of the paramagnetic magnetization in quark matter.

For completeness, in figure 6, the results of the comparison with the LQCD data are shown. The figure displays the magnetic-field dependence of renormalized magnetization  $M^r$  with and without AMM for  $T = 0.113$  GeV (left panel) and  $T = 0.176$  GeV (right panel). In the left panel,  $\kappa_i = 0.2\sigma_i^2$  leads to fairly good agreement with the LQCD data. In the right panel, the ascending trend of the magnetization of  $\kappa_i = 0.9\sigma_i^2$  with the magnetic field is close to the LQCD results. It can be concluded that the results of the nonzero AMM show a tendency approaching the LQCD data at stronger magnetic fields.

#### 4. Conclusions

In this study, the quark AMM proportional to the chiral condensate square ( $\kappa_i = v\sigma_i^2$ ) has been utilized in the PNJL model. The longitudinal and transverse pressures demonstrate the anisotropy characteristics of the strong magnetic field. The ultraviolet divergences and nonphysical oscillatory behavior were eliminated in the VMR scheme. And the renormalized magnetization of quark matter was numerically shown at finite temperature in the presence of a background magnetic field, which is crucial to account for the paramagnetism of QCD at finite temperature. At low temperatures, the presence of an AMM led to a decrease in the longitudinal pressure and an increase in the transverse pressure. Moreover, this anisotropy is enhanced by the larger scale of the AMM. However, as the temperature increased, the influence of the AMM on both the longitudinal and transverse pressures becomes insignificant.

To further explore the effect of AMMs on the paramagnetism of quark matter, we analyzed its impact on the renormalized magnetization. At low temperatures, the nonzero AMM increased the renormalized magnetization and consequently enhanced the paramagnetism of quark matter. However, as the temperature increased, the effect of the AMM on paramagnetism gradually diminished. The inflection point of the renormalized magnetization indicates the pseudocritical temperature for the chiral crossover. The comparison with LQCD data has shown that the results with nonzero AMMs are more reliable. The results are meaningful for providing the underlying connection between the paramagnetism and the chiral-phase transition of QCD.

#### Acknowledgments

The authors are grateful for the support from the National Natural Science Foundation of China under Grant Nos. 11875181 and 11705163. This work was also sponsored by the Fund for Shanxi '1331 Project' Key Subjects Construction.

#### Data availability statement

No new data were created or analysed in this study.

#### ORCID iDs

Rui He  <https://orcid.org/0009-0007-7351-3500>

Xin-Jian Wen  <https://orcid.org/0000-0001-9188-3539>

## References

- [1] Duncan R C and Thompson C 1992 *Astrophys. J. Lett.* **392** L9
- [2] Paczynski B 1992 *Acta Astron.* **42** 145–53
- [3] Taylor J H, Manchester R N and Lyne A G 1993 *Astrophys. J. Suppl.* **88** 529–68
- [4] Thompson C and Duncan R C 1996 *Astrophys. J.* **473** 322
- [5] Melatos A 1999 *Astrophys. J. Lett.* **519** L77
- [6] Ibrahim A I *et al* 2004 *AIP Conf. Proc. The Discovery of a Transient Magnetar 714* 294–7
- [7] Vachaspati T 1991 *Phys. Lett. B* **265** 258–61
- [8] Campanelli L 2013 *Phys. Rev. Lett.* **111** 061301
- [9] Canuto V and Chiu H Y 1968 *Phys. Rev.* **173** 1210–9
- [10] Canuto V and Chiu H Y 1968 *Phys. Rev.* **173** 1220–8
- [11] Canuto V and Chiu H Y 1968 *Phys. Rev.* **173** 1229–35
- [12] Chiu H Y, Canuto V and Fassio-Canuto L 1968 *Phys. Rev.* **176** 1438–42
- [13] Fushiki I, Gudmundsson E H, Yngvason J and Pethick C J 1992 *Annals Phys.* **216** 29–72
- [14] Chakrabarty S 1996 *Phys. Rev. D* **54** 1306–16
- [15] Chakrabarty S, Bandyopadhyay D and Pal S 1997 *Phys. Rev. Lett.* **78** 2898–901
- [16] Bandyopadhyay D, Chakrabarty S and Pal S 1997 *Phys. Rev. Lett.* **79** 2176–9
- [17] Thorolfsson A, Rognvaldsson O E, Yngvason J and Gudmundsson E H 1998 *Astrophys. J.* **502** 847
- [18] Chaichian M, Masood S S, Montonen C, Perez Martinez A and Perez Rojas H 2000 *Phys. Rev. Lett.* **84** 5261–4
- [19] Acharyya ACTA *et al* 2021 *JCAP* **01** 057
- [20] Broderick A, Prakash M and Lattimer J M 2000 *Astrophys. J.* **537** 351
- [21] Avancini S S, Menezes D P, Pinto M B and Providencia C 2012 *Phys. Rev. D* **85** 091901
- [22] Dexheimer V, Negreiros R, Schramm S and Hempel M 2013 *AIP Conf. Proc. Deconfinement to quark matter in neutron stars - The influence of strong magnetic fields 1520* 264–9
- [23] Lopes L L and Menezes D P 2012 *Braz. J. Phys.* **42** 428
- [24] Avancini S S, Menezes D P and Providencia C 2011 *Phys. Rev. C* **83** 065805
- [25] Ryu C Y, Maruyama T, Kajino T, Mathews G J and Cheoun M K 2012 *Phys. Rev. C* **85** 045803
- [26] Dexheimer V, Negreiros R and Schramm S 2012 *Eur. Phys. J. A* **48** 189
- [27] Bali G S, Bruckmann F, Endrodi G, Gruber F and Schaefer A 2013 *JHEP* **2013** 130
- [28] Ferrer E J, de la Incera V, Keith J P, Portillo I and Springsteen P L 2010 *Phys. Rev. C* **82** 065802
- [29] Khalilov V R 2002 *Phys. Rev. D* **65** 056001
- [30] Chatterjee D, Elghozi T, Novak J and Oertel M 2015 *Mon. Not. Roy. Astron. Soc.* **447** 3785
- [31] Noronha J L and Shovkovy I A 2012 *Phys. Rev. D* **76** 105030 [erratum: *Phys. Rev. D* 86, 049901 (2012)]
- [32] Martinez A P, Rojas H P and Mosquera Cuesta H J 2003 *Eur. Phys. J. C* **29** 111–23
- [33] Ferrer E J, de la Incera V, Manreza Paret D, Pérez Martínez A and Sanchez A 2015 *Phys. Rev. D* **91** 085041
- [34] Sinha M, Huang X G and Sedrakian A 2013 *Phys. Rev. D* **88** 025008
- [35] Singh J P 1985 *Phys. Rev. D* **31** 1097–108
- [36] Bicudo P J A, Ribeiro J E F T and Fernandes R 1999 *Phys. Rev. C* **59** 1107–12
- [37] Strickland M, Dexheimer V and Menezes D P 2012 *Phys. Rev. D* **86** 125032
- [38] Fayazbakhsh S and Sadooghi N 2014 *Phys. Rev. D* **90** 105030
- [39] Wen X J, He R and Liu J B 2021 *Phys. Rev. D* **103** 094020
- [40] He R and Wen X J 2022 *Phys. Rev. D* **106** 116023
- [41] Mao S 2022 *Phys. Rev. D* **106** 034018
- [42] Mei J and Mao S 2020 *Phys. Rev. D* **102** 114035
- [43] D’Elia M and Negro F 2011 *Phys. Rev. D* **83** 114028
- [44] Kawaguchi M and Huang M 2023 *Chin. Phys. C* **47** 064103
- [45] Xu K, Chao J and Huang M 2021 *Phys. Rev. D* **103** 076015
- [46] Ferrer E J, de la Incera V, Portillo I and Quiroz M 2014 *Phys. Rev. D* **89** 085034
- [47] Avancini S S, Farias R L S, Scoccola N N and Tavares W R 2019 *Phys. Rev. D* **99** 116002
- [48] Avancini S S, Farias R L S, Pinto M B, Restrepo T E and Tavares W R 2021 *Phys. Rev. D* **103** 056009
- [49] Tavares W R, Farias R L S, Avancini S S, Timóteo V S, Pinto M B and Krein G 2021 *Eur. Phys. J. A* **57** 278

- [50] Farias R L S, Tavares W R, Nunes R M and Avancini S S 2022 *Eur. Phys. J. C* **82** 674
- [51] Chaudhuri N, Ghosh S, Roy P and Sarkar S 2022 *Phys. Rev. D* **106** 056020
- [52] Chaudhuri N, Ghosh S, Sarkar S and Roy P 2019 *Phys. Rev. D* **99** 116025
- [53] Ratti C, Thaler M A and Weise W 2006 *Phys. Rev. D* **73** 014019
- [54] Chaudhuri N, Ghosh S, Sarkar S and Roy P 2020 *Eur. Phys. J. A* **56** 213
- [55] Schwinger J S 1948 *Phys. Rev.* **73** 416–7
- [56] Hatsuda T and Kunihiro T 1994 *Phys. Rept.* **247** 221–367
- [57] Bali G S, Bruckmann F, Endrodi G and Schafer A 2014 *Phys. Rev. Lett.* **112** 042301